MATHEMATICAL BIOSCIENCES
AND ENGINEERING
Volume **4**, Number **1**, January **2007**

http://www.mbejournal.org/

pp. **113–129**

THE STABILITY OF STATIONARY FRONTS FOR A DISCRETE NERVE AXON MODEL

Christopher E. Elmer
High Bridge, NJ 08829, USA

Abstract. We consider the stability of single-front stationary solutions to a spatially discrete reaction-diffusion equation which models front propagation in a nerve axon. The solution's stability depends on the coupling parameter, changing from stable to unstable and from unstable to stable at a countably infinite number of values of this diffusion coefficient.

1. **Introduction.** The discrete Nagumo equation, a reaction-diffusion equation with a bistable reaction term, $f(u)$, and a discrete diffusion term (1), has stationary front solutions connecting the "stable" equilibria of the nonlinearity even though the integral of the nonlinearity from one equilibrium to the other, $\int f(u)\,du$, is not zero, as long as diffusion strength is weak enough. When they exist, these stationary fronts typically exist in pairs, one stable and one unstable to local perturbations, and the existence of these solutions is often referred to as *propagation failure*. When comparing the energy of the two solutions (when evaluating the action of the maps) one solution typically has a higher value than the other, providing a barrier to motion, where the stationary front with the smaller energy (smaller value of the action) is the stable one of the two. The bistable nonlinearity (2) used in this work contains a detuning parameter which allows us to vary the value of $\int f(u)\,du$ from $(-1/4, 1/4)$. It is shown in [12] that the detuning parameter can be chosen so that propagation failure exists for almost all positive values of the diffusion coefficient, the coefficient which specifies strength of the discrete diffusion.

In this work we apply the Evans [20] function technique adapted [4] to our discrete system, with the zigzag nonlinearity (2), to discover whether a stationary front solution is linearly stable. As we will see, solution stability depends on the strength of the discrete diffusion term. The works [3, 5, 31, 32, 33] provide a detailed overview of the implementation of the Evans function for continuous diffusion.

Saltatory conduction is the rapid propagation of action potentials along myelinated axons. Quoting [23]: "Even though ions cannot flow significantly through the thick myelin sheaths of myelinated nerves, they can flow with considerable ease through the nodes of Ranvier. Therefore, action potentials can occur only at the nodes. Yet, the action potentials are conducted from node to node; this is called saltatory conduction. That is, electrical current flows through the surrounding extracellular fluids outside the myelin sheath and also through the axoplasm from node to node, exciting successive nodes one after another. Saltatory conduction is of value for two reasons. First, by causing the depolarization process to jump long intervals along the axis of the nerve fiber, this mechanism increases the velocity

2000 *Mathematics Subject Classification.* 34K20,37K45.

Key words and phrases. bistable, spatially discrete, reaction-diffusion, Evans function, stability, perturbation.

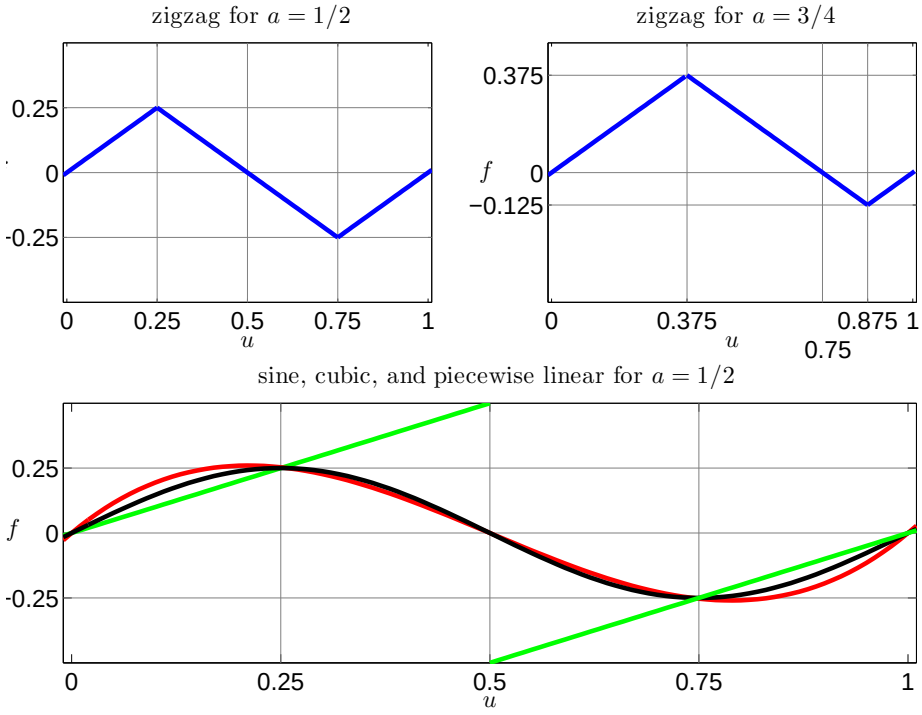

FIGURE 1. The top two plots are of the nonlinearity $f(u, a)$ (2) for $a = 1/2$ and $a = 3/4$. The bottom plot is of frequently studied nonlinearities that when used in (1) the single front stationary solutions demonstrate similar characteristics to each other, such as propagation failure and off-centered stability. $f = .25\sin(2\pi u)$ is in black, $f = 5.4u(u-.5)(u-1)$ is in red, and $f = u - h(u-.5)$ (where h is the unit step function) is in green.

of nerve transmission in myelinated fibers as much as 5-fold to 50-fold. Second, saltatory conduction conserves energy for the axon, for only the nodes depolarize, allowing perhaps a hundred times smaller loss of ions than would otherwise be necessary and therefore requiring little metabolism for re-establishing the sodium and potassium concentration difference across the membrane after a series of nerve impulses." The mathematical model of a myelinated axon that we use here comes from postulating an equivalent electrical circuit model (cable theory) of the excitable axonal membrane. The following is adapted from [25]. Consider a single nerve fiber (axon) coated with myelin with periodically spaced gaps (nodes). Assuming the axial currents are constant, the intracellular, I_i, and the extracellular, I_e, currents between two consecutive nodes are (by Ohm's law)

$$L_n r_i I_{i,n} = -(u_{i,n+1} - u_{i,n}), \qquad \text{and} \qquad L_n r_e I_{e,n} = -(u_{e,n+1} - u_{e,n}),$$

where L_n is the length of the myelin sheath between the n^{th} and $(n+1)^{st}$ nodes, r_i and r_e are the intracellular and extracellular resistances per unit length of material, and $u_{i,n}$ and $u_{e,n}$ are the intracellular and extracellular voltages in the n^{th} node.

Using Kirchoff's laws, one obtains

$$I_{i,n-1} - I_{i,n} = I_{e,n} - I_{e,n-1} = \mu_n p \left(C \frac{\partial u_n}{\partial t} + I_{ion,n} \right),$$

where the quantities in the parentheses are the capacitive current and the ionic current flowing through the n^{th} node from inside to outside, $u_n = u_{i,n} - u_{e,n}$, μ_n is the length of the n^{th} node, p is the perimeter length of the axon (assumed to be constant for now), C is the capacitance, and $I_{ion,n}$ is the ionic current at each node. Thus the total transmembrane current at a node n is given by

$$p \left(C \frac{\partial u_n}{\partial t} + I_{ion,n} \right) = \frac{1}{\mu_n (r_e + r_i)} \left(\frac{u_{n+1} - u_n}{L_n} + \frac{u_{n-1} - u_n}{L_{n-1}} \right).$$

The change of variables $\tau = t/(CR)$ nondimensionalizes time (where R has units Ωcm^2) and we obtain

$$\frac{\partial u_n}{\partial \tau} = \rho_n \left(\frac{u_{n+1} - u_n}{L_n} + \frac{u_{n-1} - u_n}{L_{n-1}} \right) - R I_{ion,n},$$

where $\rho_n = R/(\mu_n p(r_i + r_e))$. This is a description of the leading edge of the pulse which travels down a myelinated nerve axon. To be complete, one also needs to consider the dynamics of the trailing edge, i.e., how the nerve "resets" itself. We consider this leading edge model here. We now let the length of each node $\mu_n = \mu$ and the distance between each node $L_n = L$ for all n, we set $f(u_n, a) = R I_{ion,n}$, we set $d = \rho_n / L$, and for convenience we rename τ as t.

Thus in this work we consider the stability of the single front monotone stationary solutions to

$$\dot{u}_n(t) = d[u_{n+1}(t) - 2u_n(t) + u_{n-1}(t)] - f(u_n(t), a), \tag{1}$$

where we choose the nonlinearity f to be

$$f(u, a) = \begin{cases} u, & u < a/2, \\ a - u, & a/2 \le u \le (a+1)/2, \\ u - 1, & u > (a+1)/2, \end{cases} \tag{2}$$

and apply the boundary conditions $u_{-\infty} \equiv \lim_{n \to -\infty} u_n = 0$ and $u_{\infty} \equiv \lim_{n \to \infty} u_n = 1$ (connecting the "stable" equilibria of f) where $n \in \mathbb{Z}$, $t \ge 0$, and $a \in (0, 1)$, and where we set $\dot{u}_n(t) = \frac{d}{dt} u_n(t) = 0$ for all $n \in \mathbb{Z}$ and $t \ge 0$. Thus the solutions being considered in this paper are monotone increasing doubly infinite sequences between 0 and 1, which we write as $\{u_n\}_{n=-\infty}^{\infty}$ or abbreviate as $\{u_n\}$.

When considering traveling wave solutions to (1), of particular interest is the phenomenon of propagation failure, the effective resistance due to the discreteness of the diffusion operator. The most commonly used reaction terms (nonlinearities) are the sine [1, 2, 4, 9] and the cubic [7, 15, 24, 28, 30, 38, 39, 40] functions, as well as the piecewise linear caricature of these nonlinearities [8, 14, 16, 17, 21, 29, 34] (bottom plot of Figure 1). For these commonly used bistable nonlinearities, when the system's parameters are such that fronts fail to propagate (for instance, when the integral of the nonlinearity is zero when integrated over the range of the dependent variable), there exist two stationary single front monotone solutions, one stable and one unstable. For the sine, the cubic, and the piecewise linear nonlinearities, it is generally believed that the solution centered with respect to its range is unstable, while the solution off-centered is stable.

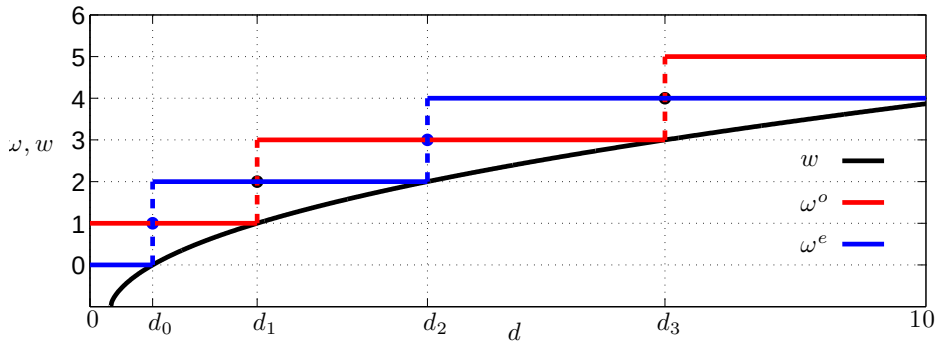

FIGURE 2. The ω versus d plot illustrating equations (3) and (4). The function $w(d)$ is in black, ω^o is in red, and ω^e is in blue.

What makes the spatially discrete bistable reaction-diffusion equation (1) with nonlinearity (2) draw our interest (the contribution of this paper) is that, as d is increased from 0 to ∞, the stability of the monotone stationary fronts changes i.e., unstable fronts become stable and stable fronts become unstable. The values of d at which the stability changes occur are isolated, and there are a countably infinite number of them. This is atypical behavior even though (2) can be considered as being in the same class as the more commonly used nonlinearities listed above. Since often when modeling the nonlinearities chosen to represent the observed bistable behavior are zeroth-order approximations (or first-order at best), our intent is to point out that additional care may be needed. However since (1) with (2) only models the leading-edge behavior (a heteroclinic orbit) the applicability of our model to actual action potential propagation (a homoclinic orbit) is limited.

This paper is organized into two sections and a conclusion. We begin in Section 2 with definitions and applicable results concerning the stationary monotone front solutions to (1) with (2), results that follow from [12]. Next in Section 3 we perturb the solution and derive the associated Evans function, which we use to state various stability results. In the conclusion we summarize our results and discuss simple extensions.

2. **Background: solutions.** This section provides some necessary background about the single stationary monotone front solutions to (1) with (2), details of which can be found in [12]. Up to translation, for $a = 1/2$ there are at least two stationary single front solutions for all $d \geq 0$ and at most two solutions for almost all $d \geq 0$. The monotone front solutions can be classified by the number of elements, the number of u_n, of the solution $\{u_n\}$ that lie in the interval $[a/2, (a+1)/2]$, i.e., the middle section of (2).

DEFINITION 2.1. *Let $\omega \in \mathbb{Z}^+ \cup \{0\}$ be the number of elements of $\{u_n\}$ in $[a/2, (a+1)/2]$. In addition, let $\omega^e = \omega$ when ω is even and $\omega^o = \omega$ when ω is odd.*

DEFINITION 2.2. *Let $\{u_n^e\} = \{u_n\}$ when ω is even and $\{u_n^o\} = \{u_n\}$ when ω is odd.*

Figure 3 illustrates both $\{u_n^e\}$ and $\{u_n^o\}$ for values of u_n near the interface for $d \in [0, 10]$. Since the diffusion coefficient d is a measure of the interface thickness,

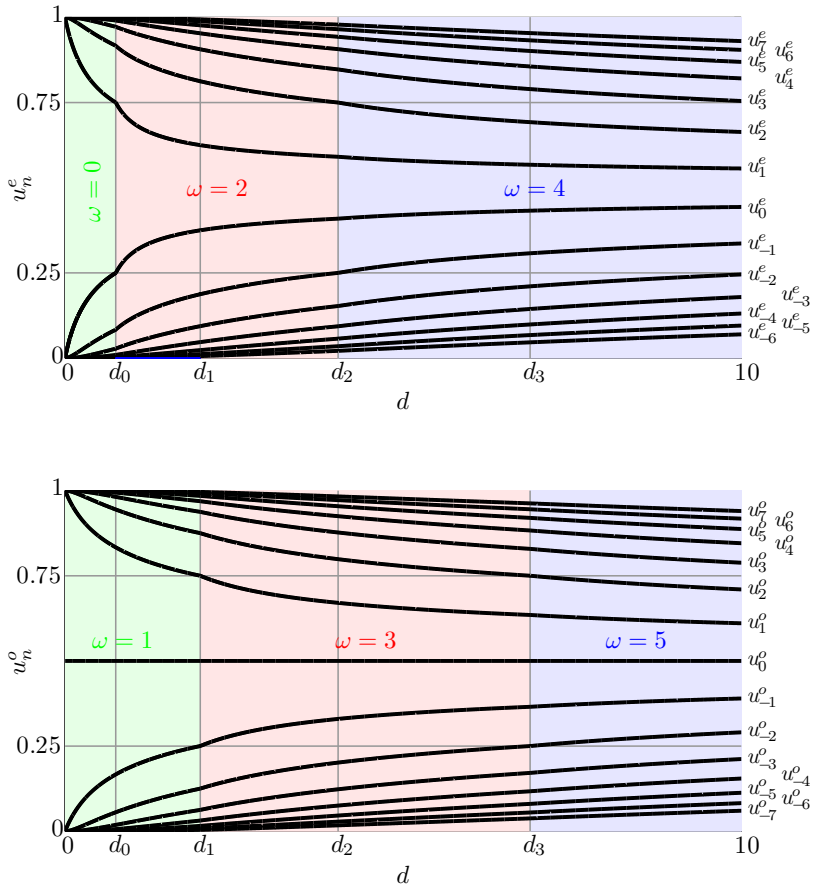

FIGURE 3. Plots of u_n versus d for the off-centered (ω even) and centered (ω odd) solutions with $a = 1/2$ for values of u_n at the interface. Here $a/2 = 1/4$ and $(a+1)/2 = 3/4$.

we should expect that ω is a function of d. In fact, for $d \geq 3/4$, the even and odd ω's are defined by the equations

$$\omega^e(d) = 2\,\mathrm{Int}\,(\rho) + 2 \quad \text{and} \quad \omega^o(d) = 2\,\mathrm{Int}\left(\rho + \frac{1}{2}\right) + 1, \tag{3}$$

$$\text{where} \quad \rho = \frac{1}{\kappa}\left[\tan^{-1}\left(\frac{2-\sqrt{4d+1}}{\sqrt{4d-1}}\right)\right] \quad \text{with} \quad \kappa = -\left|\cos^{-1}\left(1-\frac{1}{2d}\right)\right|,$$

and $\mathrm{Int}(x)$ is the integer obtained from x when truncating. For $d \in [0, 3/4)$, $\omega^e(d) = 0$ and $\omega^o(d) = 1$. The relations (3) partition the interval for d, $[0, \infty)$, in terms of ω. When $a = 1/2$, the solutions $\{u_n^e\}$ and $\{u_n^o\}$ satisfy the symmetry conditions $u_n^e = 1 - u_{1-n}^e$ and $u_n^o = 1 - u_{-n}^o$ for almost every $d \geq 0$. As it turns out, this implies that for $a = 1/2$, as d increases to a value such that ω increases, ω must increase by two (Figures 3 and 2).

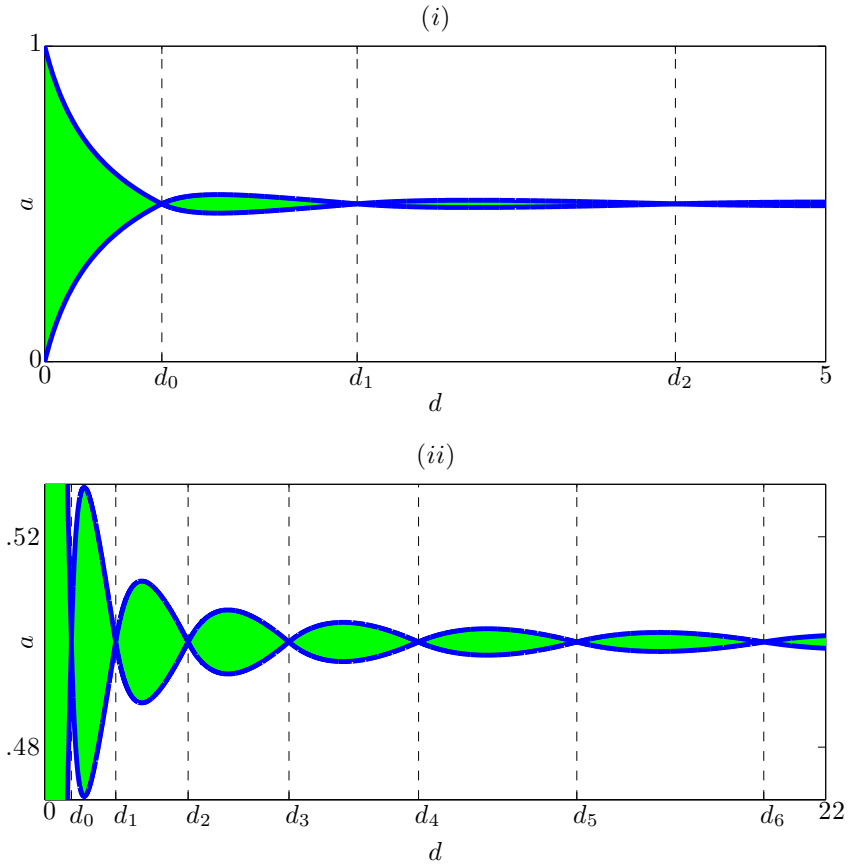

FIGURE 4. Two views of the a versus d plot. The shaded regions and the blue lines show the values of (a, d) for which stationary single front solutions exist (propagation failure). The values of d_ω, the values of d for which there is no propagation failure, are marked.

DEFINITION 2.3. *Let d_ω be the value of d where ω increases by 2, i.e., for a fixed ω, the value of d for which $\rho \in \mathbb{Z}^+ \cup \{-1, 0\}$ (ω even) or $\rho + 1/2 \in \mathbb{Z}^+ \cup \{0\}$ (ω odd).*

DEFINITION 2.4. *Let $\mathcal{D} = \{d_\omega\}_0^\infty$.*

REMARK 2.1. *The above definitions imply that $\omega = w(d_\omega)$, where*

$$w(d) \equiv \frac{2}{\kappa}\left[\tan^{-1}\left(\frac{2-\sqrt{4d+1}}{\sqrt{4d-1}}\right)\right]. \tag{4}$$

See Figure 2. The function $w(d)$ is monotone increasing and unbounded at infinity i.e., $\lim_{d\to\infty} w(d) = \infty$. Thus there are an infinite (countably) number values of d_ω in $\mathcal{D}$ and $\omega \in \mathbb{Z}^+ \cup \{0\}$.

As a demonstration of the partitioning, the first six values of d_ω for the off-centered solution $\{u_n^e\}$ are,

ω^e	0 | 2	2 | 4	4 | 6	6 | 8	8 | 10	10 | 12
d_ω	3/4	~ 4.037	~ 10.530	~ 20.258	~ 33.228	~ 49.440
	d_0	d_2	d_4	d_6	d_8	d_{10}

The first six for the centered solution $\{u_n^o\}$ are,

ω^o	1 | 3	3 | 5	5 | 7	7 | 9	9 | 11	11 | 13
d_ω	2	~ 6.879	~ 14.989	~ 26.338	~ 40.929	~ 58.762
	d_1	d_3	d_5	d_7	d_9	d_{11}

Thus if $d = 3.1$, then for the solution $\{u_n^e\}$, $3.1 = d \in [d_0, d_2) = [3/4, \sim 4.037)$, and it has 2 elements in $[1/4, 3/4]$ (u_0^e and u_1^e) i.e., $\omega = 2$. For the solution $\{u_n^o\}$, $3.1 = d \in [d_1, d_3) = [2, \sim 6.879)$, and it has 3 elements in $[1/4, 3/4]$ (u_{-1}^o, u_0^o, and u_1^o) i.e., $\omega = 3$.

Until this point we have focused on when $a = 1/2$. Using the implicit function theorem, it can be shown that the two stationary solutions persist as a is perturbed from $1/2$ at all values of $d \geq 0$ such that $d \notin \mathcal{D}$. For $d \in \mathcal{D}$, stationary monotone front solutions exist only when $a = 1/2$ and there are an infinite number of them. This is because the heteroclinic connection becomes integrable for $d \in \mathcal{D}$. Figure 4 illustrates the values of a for which these solutions exist. For (d, a) in the shaded region, we have two stationary monotone single-front solutions to (1) with (2). For (d, a) on the boundary of the shaded region, the two solutions come together into one. For (d, a) outside of the shaded region, no stationary monotone single-front solutions exist. Figure 8 shows solutions plotted on the real axis for five values of d, of which two ($d_1 = 2$ and $d_2 \approx 4.0377$) are in $\mathcal{D}$. For the three $d \notin \mathcal{D}$, the two solutions are shown on separate plots and we see that they consist of discrete steps from 0 to 1. For the two $d \in \mathcal{D}$, instead in a discrete stepping, we have a continuous curve from zero to one with the centered and the off-centered solutions marked along the curve. Besides these two solutions, the curve defines a solution for every choice of $u_0 \in (0, 1)$.

3. **A discrete Evans function.**

Our stability results are obtained by evaluating the leading eigenvalue of the linearization of (1) about its solutions $\{u_n^o\}$ and $\{u_n^c\}$. We proceed by deriving a discrete Evans function (see [4] for another example) and use it to explicitly state stability results for the single front monotone solutions to (1) with (2). Simply put, we now perturb the solution and look for unstable modes.

3.1. **The perturbation.**

We let

$$\{y_n(t)\} = \{u_n\} + \{\delta_n(t)\}$$

with $|\delta_n(t)| \leq \min(|u_n - a/4|, |u_n - (a+1)/4|)$ and substitute into (1) with (2) to obtain the system of equations defined by

$$\dot{\delta}_n(t) = d[\delta_{n+1}(t) - 2\delta_n(t) + \delta_{n-1}(t)] + \begin{cases} \delta_n(t), & |m| \leq (\omega-1)/2, \\ -\delta_n(t), & |m| > (\omega-1)/2, \end{cases}$$

where $m = n - 1/2$ if ω is even and $m = n$ if ω is odd. Thus the following exploration for λ is valid as long as the solution $\{u_n\}$ has no values equal to $a/2$ or $(a+1)/2$.

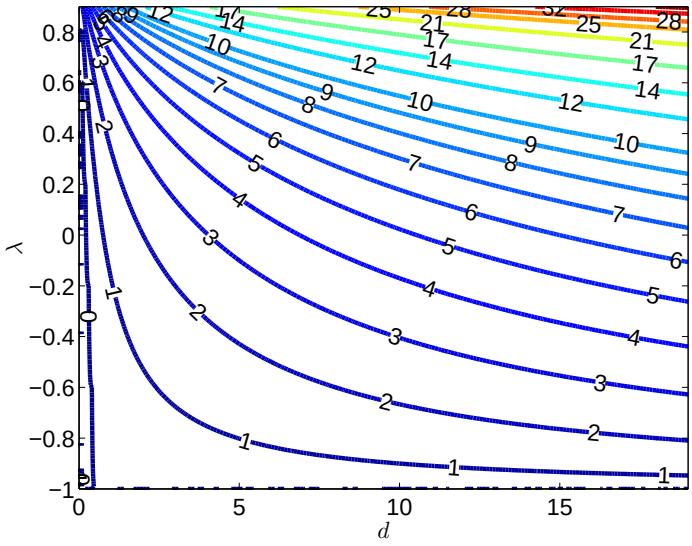

FIGURE 5. Contour plot where each contour line is a fixed value of ω_λ, as defined by (7). We observe that λ decreases as d increases.

We now separate variables and assume we can write $\delta_n(t) = v_n \alpha e^{\lambda t}$, substitute, and obtain

$$\begin{cases} 0 = dv_{n+1} - (2d + \lambda - 1)v_n + dv_{n-1}, & |m| \le (\omega - 1)/2, \\ 0 = dv_{n+1} - (2d + \lambda + 1)v_n + dv_{n-1}, & |m| > (\omega - 1)/2. \end{cases} \tag{5}$$

Solving for v_n, on each of the intervals (the middle interval $|m| \le (\omega - 1)/2$ and the left- and right-hand tails $|m| > (\omega - 1)/2$) any monotone solution of (5) is of the form

$$v_n = \begin{cases} A_+\sigma_+^m + A_-\sigma_-^m, & m < -(\omega - 1)/2, \\ C_+\nu_+^m + C_-\nu_-^m, & -(\omega - 1)/2 \le m \le (\omega - 1)/2, \\ B_+\sigma_+^m + B_-\sigma_-^m, & m > (\omega - 1)/2, \end{cases} \tag{6}$$

where

$$\sigma_\pm = \frac{2d + \lambda + 1}{2d} \pm \frac{\sqrt{\lambda + 1}\sqrt{\lambda + 1 + 4d}}{2d}$$

and

$$\nu_\pm = \frac{2d + \lambda - 1}{2d} \pm \frac{\sqrt{\lambda - 1}\sqrt{\lambda - 1 + 4d}}{2d}.$$

Using the four matching equations generated by satisfying (5) where the intervals meet (coupling the solution pieces from each interval together), A_+ and A_- can be expressed as functions of B_+, B_-, and λ; or B_+ and B_- can be expressed as functions of A_+, A_-, and λ. We desire that the boundary conditions $\lim_{|n|\to\infty} v_n = 0$ be satisfied, which implies that A_- must equal zero since $\sigma_- \in (0, 1)$ and B_+ must equal zero since $\sigma_+ = \sigma_-^{-1} > 1$. If we set $A_- = 0$, we can write B_+ as a function of

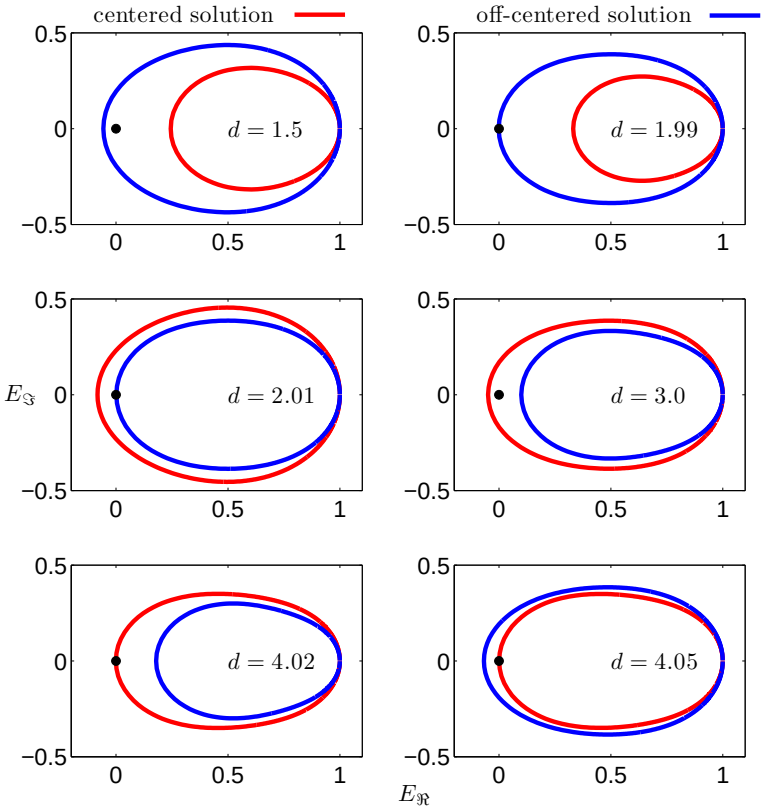

FIGURE 6. Plot of the E for $\lambda \in (-i\infty, i\infty)$. The centered solutions are in red and the off-centered solutions are in blue. An unstable mode is present when the curve encloses the origin.

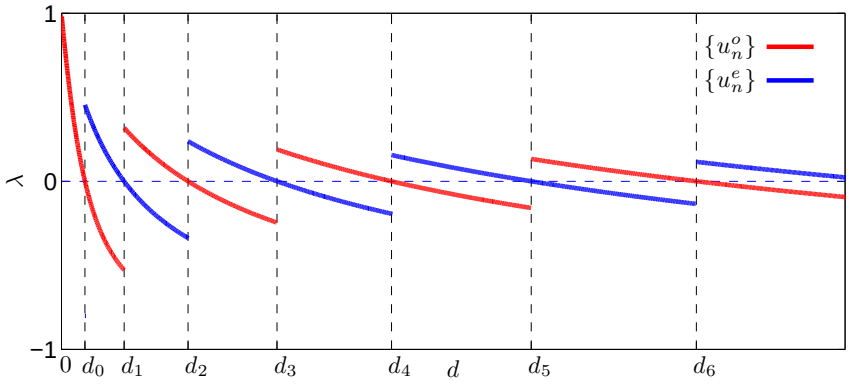

FIGURE 7. Plot of the λ values such that $\Re(\lambda) > -1$ with respect to d. The centered solutions λ are in red and the off-centered solutions λ are in blue.

A_+ and λ i.e.,

$$B_+(d,\omega) = \begin{cases} \dfrac{1+\sigma_-}{2(1+\sigma_+^2)}A_+, & \omega = 0, \\ \dfrac{\sigma_-^{\omega-1}}{(\nu_+-\nu_-)(\sigma_+-\sigma_-)}[\nu_+^{\omega-1}(\sigma_- - \nu_+)^2 - \nu_-^{\omega-1}(\sigma_- - \nu_-)^2]A_+, & \omega > 0, \end{cases}$$

which has branch points at $\lambda = -1, -1-4d$, for $\omega > 0$, where the integer valued ω is defined by (3). Again, our goal is for $B_+ = 0$. If A_+ were to equal zero, then $v_n = 0$ for all n, hence $\delta_n(t)$ would be zero for all n and $t > 0$. Thus assuming that $A_+ \neq 0$ gives us the eigenvalue problem "for what values of λ does $B_+ = 0$." Let λ_0 be the leading eigenvalue for our problem. Then our solutions are linearly stable when $\lambda_0 < 0$ and linearly unstable when $\lambda_0 > 0$. Figure 7 illustrates λ_0 where we can see that the stability of our two solutions changes at specific isolated values of d.

REMARK 3.1. *A formal explanation of the behavior that the stability of the two stationary monotone front solutions vary with d is that although ω is an increasing function of d, λ_0 is monotone increasing in ω while λ_0 is monotone decreasing in d. To see this we set $B_+(d,\omega_\lambda) = 0$ and solve for ω to obtain*

$$\begin{aligned} \omega_\lambda(d,\lambda) &= \frac{2}{\kappa_\lambda}\left[\tan^{-1}\left(\frac{2-\sqrt{4d+1+4d\lambda+2\lambda+\lambda^2}}{\sqrt{4d-1-4d\lambda+2\lambda-\lambda^2}}\right)\right]+1 \qquad (7) \\ &= \frac{2}{\kappa_\lambda}\left[\tan^{-1}\left(\frac{\sigma_- - \cos(\kappa_\lambda)}{\sin(\kappa_\lambda)}\right)\right]+1 \end{aligned}$$

where

$$\kappa_\lambda = -\left|\cos^{-1}\left(1+\frac{\lambda-1}{2d}\right)\right|.$$

Differentiating, we find that

$$\begin{aligned} \frac{\partial}{\partial\lambda}\omega_\lambda &= \frac{2}{\kappa}\frac{\sin^2(\kappa_\lambda)}{1+\sigma_-^2-2\sigma_-\cos(\kappa_\lambda)}\frac{\partial}{\partial\lambda}\left(\frac{\sigma_- - \cos(\kappa_\lambda)}{\sin(\kappa_\lambda)}\right) \\ &\quad -\frac{2}{\kappa_\lambda^2}\tan^{-1}\left(\frac{\sigma_- - \cos(\kappa_\lambda)}{\sin(\kappa_\lambda)}\right)\frac{\partial}{\partial\lambda}\kappa_\lambda > 0 \end{aligned}$$

and hence $\partial\lambda/\partial\omega > 0$, where

$$\begin{aligned} &\frac{\partial}{\partial\lambda}\left(\frac{\sigma_- - \cos(\kappa_\lambda)}{\sin(\kappa_\lambda)}\right) \\ &\quad = 2\frac{1-\lambda^2-4d\lambda-8d^2+(\lambda-1+2d)\sqrt{4d+1+4d\lambda+2\lambda+\lambda^2}}{\sqrt{4d+1+4d\lambda+2\lambda+\lambda^2}(4d-1-4d\lambda+2\lambda-\lambda^2)^{3/2}} \qquad \text{and} \\ &\frac{\partial}{\partial\lambda}\kappa_\lambda = \frac{-1}{\sqrt{4d-1-4d\lambda+2\lambda-\lambda^2}}. \end{aligned}$$

Using (7) to show that $\partial\lambda/\partial d < 0$ proves to be bit more difficult and thus instead of an algebraic verification we have included Figure 5, which shows the $\lambda(d)$ level curves for different fixed values of ω_λ.

We now explore the relationship between d and the sign of λ_0 in more detail. Since the value of $A_+ \neq 0$ is unimportant to this study, we set $E(\lambda) = B_+(A_+,\lambda)$ when $A_+ = 1$ and examine E. The Evans function $E(\lambda)$ is analytic for $\Re\lambda > -1$

when $\omega > 0$ and for $\Re\lambda > 0$ when $\omega = 0$. Thus by the argument principle, for the appropriate choice of $\Re\lambda$ fixed, with $\mathcal{C}$ enclosing the region of λ to the right of $\Re\lambda$

$$\begin{aligned}\frac{1}{2\pi i}\int_{\mathcal{C}} \frac{dE}{d\lambda}\frac{d\lambda}{E} = \frac{1}{2\pi i}\int_{\Re\lambda - i\infty}^{\Re\lambda + i\infty} \frac{dE}{d\lambda}\frac{d\lambda}{E} &= \text{Number of zeros in } \mathcal{C} \qquad (8)\\ &= \text{Number of winds around 0 in the } (E_{\Re}, E_{\Im}) \text{ plane}\\ &\quad \text{as } \Im\lambda \text{ goes from } -\infty \text{ to } \infty,\end{aligned}$$

where $E_{\Re}$ is the real part of E and $E_{\Im}$ is the imaginary part of E.

We now list some properties of E.

- For $\omega > 0$, $\lim_{\Re\lambda \to -1^+} \frac{1}{2\pi i}\int_{\Re\lambda - i\infty}^{\Re\lambda + i\infty} \frac{dE}{d\lambda}\frac{d\lambda}{E} = 1$, for $d \notin \mathcal{D}$. Figure 7 is a plot illustrating this one value of λ for $d \in [0, 25]$.
- For λ along the imaginary axis, $\lambda = ib$ for b real, the real part of E is even since $E_{\Re}(ib) = [E(ib) + E(-ib)]/2$, and the imaginary part of E is odd since $E_{\Im}(ib) = [E(ib) - E(-ib)]/2$, for $d \geq 3/4$.
- Since E is analytic along the imaginary axis and since $dE_{\Re}/d\lambda(ib)$ is odd, $E_{\Re}(ib)$ has a maximum or minimum at $b = 0$.
- Since $\lim_{|b|\to\infty} E(ib) = 1$, $\lim_{|b|\to\infty} E_{\Re}(ib) = 1$ and $\lim_{|b|\to\infty} E_{\Im}(ib) = 0$.
- For $d \geq 3/4$ and b real, $E_{\Re}(ib, d)$ increases monotonically from $b = 0$ to $b = \pm\infty$.
- $E_{\Im}(ib)$ is positive for b positive.

Since our concern is unstable modes, we consider for the contour in (8) the boundary of the region which encloses $\Re\lambda > 0$. The curve produced in the $(E_{\Re}, E_{\Im})(ib)$ plane is symmetric about the $E_{\Im}$ axis and consists of a single closed curve that goes through the point $(1, 0)$. The winding number is either zero (no unstable modes), or one (one unstable mode), depending on whether the origin is contained in the curve. Because of symmetry, this is equivalent to asking whether $E_{\Re}(0)$ is positive (winding number zero) or negative (winding number 1) see Figure 6. Since $E_{\Im}(0) = 0$,

$$\begin{aligned} E_{\Re}(0) &= E(0) = \frac{d(1+\sigma_0)\sigma_0}{2(2d+1)} \qquad \text{for} \quad \omega = 0 \qquad \text{and}\\ E_{\Re}(0) &= E(0)\\ &= \sigma_0^{\omega-1}\left[\frac{\sqrt{4d+1}-2}{\sqrt{4d+1}}\cos([\omega-1]\kappa) + \frac{2\sqrt{4d+1}-3}{\sqrt{4d-1}\sqrt{4d+1}}\sin([\omega-1]\kappa)\right]\end{aligned}$$

for $\omega > 0$, where

$$\sigma_0 = \frac{2d+1}{2d} - \frac{\sqrt{4d+1}}{2d}.$$

When $d \in (0, 3/4)$, one proceeds in a straight forward manner to find the sign of $E_{\Re}(0)$ for the single monotone front stationary solutions. The only two such solutions that occur are for $\omega = 0$ and 1. When $\omega = 0$, $E_{\Re}(0) > 0$ for $d > 0$ and when $\omega = 1$, $E_{\Re}(0) = (\sqrt{4d+1} - 2)/\sqrt{4d+1} < 0$ for $d \in (0, 3/4)$.

For the remaining values of d we use the following function to help. Because $\sigma_0^{\omega-1}/(\sqrt{4d-1}\sqrt{4d+1}) > 0$ for $d > 1/4$, investigating the sign of $E(0)$ is equivalent

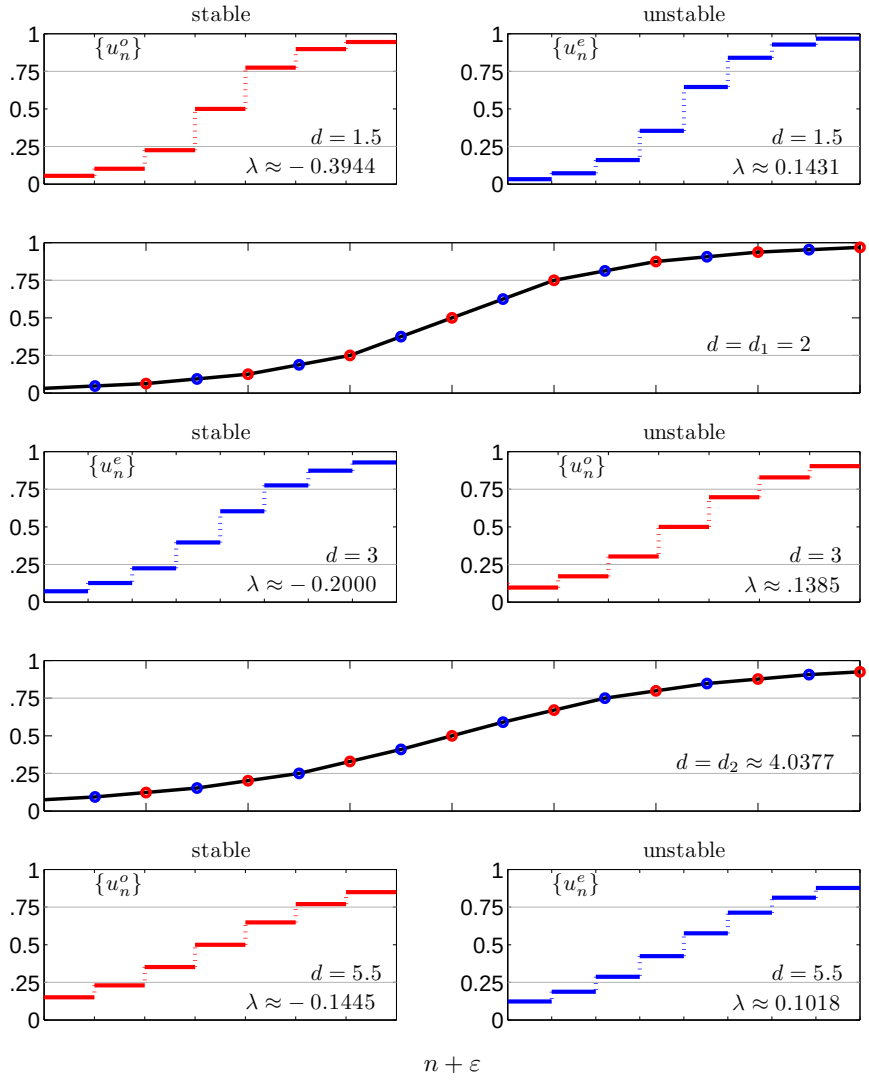

FIGURE 8. Plots of the discrete solution displayed on a continuous axis for various values of d, for $a = 1/2$. The distance between horizontal tic marks is one. The solution $\{u_n^o\}$ is in red and $\{u_n^e\}$ is in blue. The stable solutions (negative λ) are displayed on the left, the unstable (positive λ) on the right. For values of $d \in \mathcal{D}$, there exists an infinite number of monotone front solutions. In the plots for d_1 and d_2 we have marked the centered (in red) and off-centered (in blue) solutions that also exist for $d \notin \mathcal{D}$. However, the black line defines the solution for any choice of $u_0 \in (0, 1)$. See [12] for additional details.

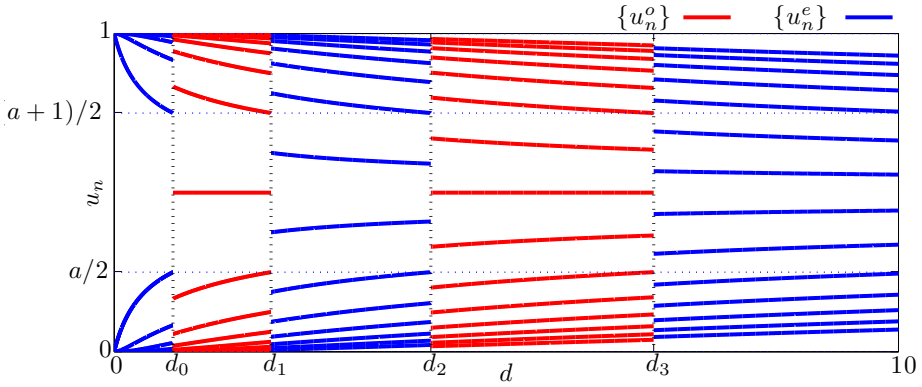

FIGURE 9. Plot of the stable solution with respect to d for $a = 1/2$. The centered solutions are in red and the off-centered solutions are in blue.

to finding the sign of

$$\mathcal{G}(d,\omega) \equiv \frac{(\sqrt{4d+1}-2)\sqrt{4d-1}}{2\sqrt{4d+1}-3} + \tan(\omega-1)\kappa,$$

which is valid for $d > 5/16$.

LEMMA 3.1. *Fix $\omega \in \mathbb{Z}^+$. Then the value of d such that $\mathcal{G} = 0$ is $d_{\omega-1}$ i.e., $\mathcal{G}(d_{\omega-1}) = 0$. In addition for $d > 5/16$, for each ω the value of d such that $\mathcal{G} = 0$ is unique.*

Proof. We begin by setting $\mathcal{G}(d,\omega_0)$ equal to zero and solving for ω_0 to obtain

$$\begin{aligned}\omega_0 &= \frac{1}{\kappa}\tan^{-1}\left(\frac{(2-\sqrt{4d+1})\sqrt{4d-1}}{2\sqrt{4d+1}-3}\right)+1 = \\ &\quad \frac{2}{\kappa}\tan^{-1}\left(\frac{2-\sqrt{4d+1}}{\sqrt{4d-1}}\right)+1 = w+1,\end{aligned} \tag{9}$$

where w is given by (4). The values of d at which w is a nonnegative integer are those contained in $\mathcal{D}$ i.e., at d_w. Since $w = \omega_0 - 1$, for fixed $\omega_0 \in \mathbb{Z}^+$ the value of d which satisfies (9) is $d = d_w = d_{\omega_0-1}$.

Taking the derivative of $\mathcal{G}(d)$, we find that

$$\mathcal{G}'(d) = \frac{4([d+1][\sqrt{4d+1}]-[3d+1])}{\sqrt{4d+1}\sqrt{4d-1}(2\sqrt{4d+1}-3)} + \left[\frac{d}{dd}(\omega-1)\kappa\right]\sec^2(\omega-1)\kappa > 0$$

for $d > 5/16$ since for $d \in [1/4,\infty)$, κ is real and increases monotonically from $-\pi$ at $d = 1/4$ to 0 for $d \to \infty$. ∎

REMARK 3.2. *Lemma 3.1 implies that the values of d at which the stability of the solution $\{u_n^e\}$ ($\{u_n^o\}$) changes are the values of d at which ω changes for $\{u_n^o\}$ ($\{u_n^e\}$).*

Furthermore, it implies that for the solution associated with each ω, when $d \in [d_{\omega-2}, d_{\omega-1})$ there exists an unstable mode, and when $d \in [d_{\omega-1}, d_\omega)$ there does not (Figure 7).

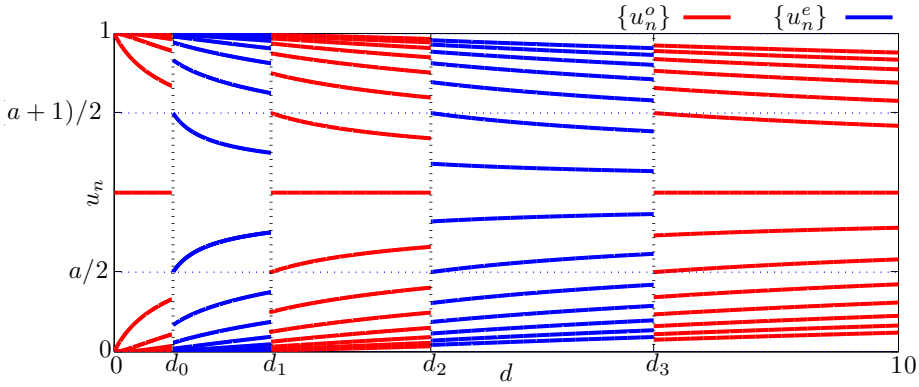

FIGURE 10. Plot of the unstable solution with respect to d for $a = 1/2$. The centered solutions are in red and the off-centered solutions are in blue.

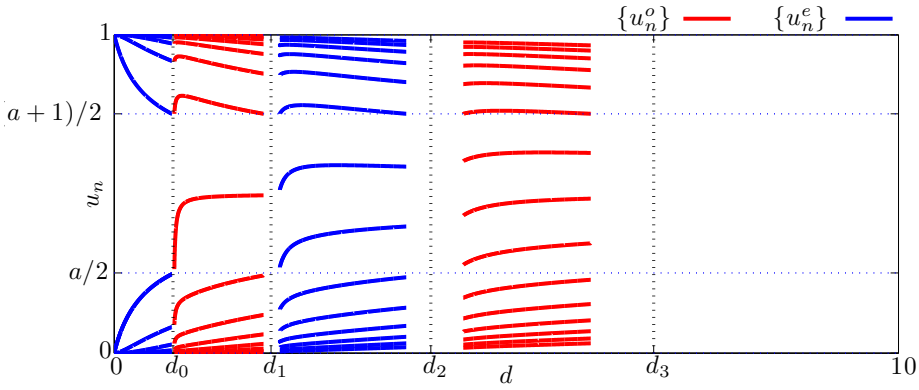

FIGURE 11. Plot of the stable solution with respect to d for $a = 0.504$. The centered solutions are in red and the off-centered solutions are in blue.

REMARK 3.3. *Equality (7) becomes equality (9) when* $\lambda = 0$.

Figure 7 illustrates the eigenvalues λ with respect to d for $\Re(\lambda) > -1$. Observe the jump in the values for one solution coincides with the zero crossing of λ for the other solution. In the plots of Figure 8 we show the stable and unstable solutions for five specific values of d. Figures 9 and 10 show the stable and unstable solutions, respectively, with respect to d for $a = 1/2$. Figure 11 pictures the stable solution with respect to d for $a = 0.502$. Notice that the solution does not exist for all $d \geq 0$ and does not exist for any $d > 6.0771$.

4. **Conclusion.** We have studied the stability of stationary single-front monotone solutions to the reaction-diffusion (1) with the zigzag-shaped piecewise linear nonlinearity (2). For $a = 1/2$, at every value of $d \geq 0$ there exist two fronts, one centered at $a = 1/2$ and one off-centered. At almost every value of $d \geq 0$, one of the fronts is stable and one is unstable, and at a countably infinite number of values of $d \geq 0$ the stability of the two solutions switch.

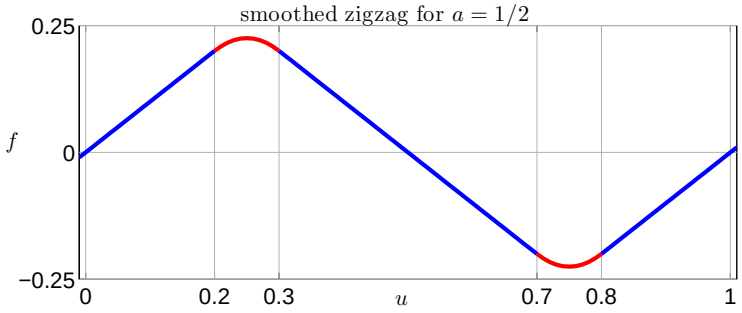

FIGURE 12. A plot of the smoothed zigzag nonlinearity (10) with $g_1 = -\left[u^2 - au + (a/2 - \delta)^2\right]/(2\delta)$ and $g_2 = \left[u^2 - (a+1)u + ((a+1)/2 - \delta)^2 - 2\delta\right]/(2\delta)$, where $\delta = 0.05$.

At the values d where the stability switching occurs, there exists a heteroclinic connection between 0 and 1 (see [13] for more detail) i.e., the two-dimensional system (map) becomes integrable. The stationary system studied here, for $a = 1/2$ and $f(u)$ (2) redefined for u outside of [0,1] to be $f(mod(u, 1))$ (making f periodic with period 1), is a standard-like map. There are a number of reactions terms that when used in (1) with $\dot{u}_n = 0$ produce integrable maps for isolated values of the coupling coefficient (for example, the standard maps of Suris [36]). For our interests the most significant consequence of the map defined by (1) with $\dot{u}_n = 0$ being integrable is that there is no lattice resistance to motion, no propagation failure due to the discreteness of the diffusion operator.

We are continuing the work in this paper along two paths. The first involves exploring the stability of stationary front solutions to (1) with other bistable nonlinearities (bistable for $u \in [0, 1]$) that are known to produce integrable maps for isolated d values. The second involves exploring the stability of the stationary monotone front solutions to $\ddot{u}_n(t) = d[u_{n+1}(t) - 2u_n(t) + u_{n-1}(t)] - f(u_n(t), a)$ which produces an Evans function with branch points on the imaginary axis at $\lambda = \pm i$ and at $\pm(1 + 4d)i$.

Our original motivation in studying nonlinearity (2) was to work with a piecewise linear approximation to the sine and cubic functions, an approximation that was in some sense better than the McKean approximation. Specifically, the potential function associated with the McKean approximation has no spinodal region. However, while the potential function which gives the nonlinearity (2) has a spinodal region, (2) does lack smoothness. We now show that this lack of smoothness is not essential for the changes in stability as d is continued. This can be seen by considering the nonlinearity

$$f(u, a) = \begin{cases} u, & u < a/2 - \delta, \\ g_1(u, a, \delta), & a/2 - \delta \le u \le a/2 + \delta, \\ a - u, & a/2 + \delta < u < (a+1)/2 - \delta \\ g_2(u, a, \delta), & (a+1)/2 - \delta \le u \le (a+1)/2 + \delta, \\ u - 1, & u \ge (a+1)/2 + \delta, \end{cases} \tag{10}$$

where $\delta \in [0, a/2) \cap [0, (a+1)/2)$. The functions g_1 and g_2 are chosen to give whatever degree of smoothness is desired to f. Figure 12 illustrates (10) for specific choices of g_1, g_2, and δ. For this demonstration we set $a = 1/2$ so that the centered

and off-centered solutions are guaranteed to exist for all $d \geq 0$ because of the symmetry of f. When $\delta = 0$, (10) equals (2). Now for $\delta > 0$ small, the solutions of (1) with (10) are exactly the same solutions of (1) with (2) for all $d \geq 0$, excluding the d within ϵ neighborhoods of the d_ω. Because the interface width increases with d, so does the size of the neighborhoods. For d large enough, the neighborhoods overlap, and we should no longer expect the solutions for the two nonlinearities to be the same.

More explicitly, suppose that $0 \leq \delta \leq 0.05$. Then for $d \in [0, .4]$ and for $d \in [.96, 1.08]$ the solutions to (1) with (2) and to (1) with (10) are the same, and so is their stability. Since these intervals lie on either side of d_0 and both intervals lie to the left of d_1, there is a least one change in stability between $d = .4$ and $d = .96$.

Acknowledgments. This work was supported in part by NSF under grant DMS-0204573.

REFERENCES

[1] K. Abell, C.E. Elmer, A.R. Humphries, and E.S. Van Vleck, "Computation of Mixed Type Functional Differential Boundary Value Problems," *SIAM J. Appld. Dyn. Sys.* **4** (2005), pp. 755-781.

[2] A.A. Aiger, A.R. Champneys, and V.M. Rothos, "A New Barrier to the Existence of Moving Kinks in Frenkel-Kontorova Lattices," *Physica D* **186** (2003), pp. 148–170.

[3] J. Alexander, R. Gardner, C. Jones, "A Topological Invariant Arising in the Stability Analysis of Travelling Waves," *J. Reine Angew. Math.* **410** (1990), pp. 167.

[4] N.J. Balmforth, R.V. Craster, and P.G. Kevrekidis, "Being Stable and Discrete," *Physica D* **135** (2000), pp. 212–232.

[5] N.J. Balmforth, R.V. Craster, S.J.A. Malham, "Unsteady fronts in an autocatalytic system," *Proc. Roy. Soc. Lond. A* **455** (1999), pp. 1401.

[6] J. Bell and C. Cosner, "Threshold Behavior and Propagation for Nonlinear Differential-Difference Systems Motivated by Modeling Myelinated Axons," *Quart. Appl. Math.* **42** (1984), 1–14.

[7] J.W. Cahn, "Theory of Crystal Growth and Interface Motion in Crystalline Materials," *Acta Met.* **8** (1960), pp. 554–562.

[8] J.W. Cahn, J. Mallet-Paret, and E.S. Van Vleck, "Traveling Wave Solutions for Systems of ODE's on a Two-Dimensional Spatial Lattice," *SIAM J. Appld. Math.* **59** (1999), pp. 455–493.

[9] A. Carpio, S.J. Chapman, S. Hastings, and J.B. Mcleod, "Wave Solutions for a Discrete Reaction-Diffusion Equation," *Eur. J Appl. Math.* **11**(2000),pp. 399–412.

[10] L.O. Chua and T. Roska, "The CNN Paradigm," *IEEE Trans. Circuit Syst.* **40** (1993), pp. 147–156.

[11] H.E. Cook, D. de Fontaine, and J.E. Hilliard, "A Model for Diffusion in Cubic Lattices and its Applications to the Early Stages of Ordering," *Acta Metallurgica 17* (1969), pp. 756–773.

[12] C.E. Elmer, "Finding Stationary Fronts for a Discrete Nagumo and Wave Equation; Construction," *Physica D* **218** (2006), pp. 11-23.

[13] C.E. Elmer, "Finding Stationary Fronts for a Spatially Discrete Bistable Parabolic and Wave Equation, Energy and Action," *in preparation.*

[14] C.E. Elmer and E.S. Van Vleck, "Analysis and Computation of Traveling Wave Solutions of Bistable Differential-Difference Equations," *Nonlinearity* **12** (1999), pp. 771–798.

[15] C.E. Elmer and E.S. Van Vleck, "A Variant of Newton's Method for the Computation of Traveling Waves of Bistable Differential-Difference Equations," *J. Dyn. and Diff. Eqns.* **14** (2002), pp. 493–517.

[16] C.E. Elmer and E.S. Van Vleck, "Traveling Waves Solutions for Bistable Differential-Difference Equations with Periodic Diffusion," *SIAM J. Appld. Math.* **61** (2001), pp. 1648–1679.

[17] C.E. Elmer and E.S. Van Vleck,"Anisotropy, Propagation Failure, and Wave Speedup in Traveling Waves of Discretizations of a Nagumo PDE," *J. Comp. Phys.* **185** (2003), pp. 562–582.

[18] G.B. Ermentrout, "Stable Periodic Solutions to Discrete and Continuous Arrays of Weakly Coupled Nonlinear Oscillators," *SIAM J. Appl. Math.* **52** (1992), pp. 1665–1687.
[19] T. Erneux and G. Nicolis, "Propagating Waves in Discrete Bistable Reaction-Diffusion Systems," *Physica D 67* (1993), pp. 237–244.
[20] J. Evans, "Nerve Axon Equations, IV: The Stable and Unstable Impulse," *Indiana Univ. Math. J.* **24** (1975), pp. 1169–1190.
[21] G. Fath, "Propagation Failure of Traveling Waves in a Discrete Medium," *Physica D* **116** (1998) 176-190.
[22] W.J. Firth, "Optical Memory and Spatial Chaos," *Phys. Rev. Lett.* **61** (1988), pp. 329–332.
[23] A. C. Guyton and J. E. Hall, *Human Physiology and Mechanisms of Disease, 6th edition* (W.B. Saunders, Philadelphia, PA, 1997).
[24] J. P. Keener, "Propagation and its Failure in Coupled Systems of Discrete Excitable Cells," *SIAM J. Appld. Math.* **47** (1987), pp. 556–572.
[25] J. Keener and J. Sneed, *Mathematical Physiology* (Springer-Verlag New York Inc., New York, NY, 1998).
[26] N. Kopell, G.B. Ermentrout, and T.L. Williams, "On Chains of Oscillators Forced at One End," *SIAM J. Appl. Math.* **51** (1991), pp. 1397–1417.
[27] J.P. Laplante and T. Erneux, "Propagation Failure in Arrays of Coupled Bistable Chemical Reactors," *J. Phys. Chem.* **96** (1992), pp. 4931–4934.
[28] R.S. MacKay and J.-A. Sepulchre, "Multistability in Networks of Weakly Coupled Bistable Units," *Physica D* **82** (1995), pp. 243–254.
[29] H. McKean, "Nagumo's Equation," *Adv. Math.* **4** (1970), pp. 209–223.
[30] J. Nagumo, S. Arimoto, and S. Yoshizawa "An Active Pulse Transmission Line Simulating Nerve Axon," *Proc. Inst. Radio Eng.* **50** (1964), pp. 2061–2070.
[31] R.L. Pego, M.I. Weinstein, "Eigenvalues and instabilities of solitary waves," *Phil. Trans Roy. Soc. A* **340** (1993) pp. 47–94.
[32] R.L. Pego, P. Smereka, M.I. Weinstein, "Oscillatory instability of traveling waves for a Kd-VBurgers equation," *Physica D* **67** (1993), pp. 45.
[33] R.L. Pego, P. Smereka, M.I. Weinstein, "Oscillatory instability of solitary waves in a continuum model of lattice vibrations," *Nonlinearity* **8** (1995), pp. 921.
[34] A.C. Scott, "Analysis of Nonlinear Distributed Systems," *Trans. IEEE CT* **9** (1962), pp. 192–195.
[35] I.E. Segal, "Nonlinear Relativistic Partial Differential Equations," *Proc. Int. Congress Math. Moscow* (1966), pp. 681–690.
[36] Y. Suris, "Integrable Mappings of the Standard Type," *Funct. Anal. Appl.* **23** (1989), pp. 74-76.
[37] R. Temam, *Infinite-Dimensional Dynamical Systems in Mechanics and Physics*, Springer-Verlag, New York, 1988.
[38] B. Zinner, "Stability of Traveling Wavefronts for the Discrete Nagumo Equation," *SIAM J. Math. Anal.* **22** (1991), pp. 1016–1020.
[39] B. Zinner, "Existence of Traveling Wavefront Solutions for the Discrete Nagumo Equation," *J. Diff. Eqn.* **96** (1992), pp. 1–27.
[40] Zeldovich and Frank-Kamenetskii, *Dokl. Akad. Nauk SSSR* **19** (1938) pp. 693–697.

Received on April 15, 2006. Revised on August 15, 2006.

E-mail address: chris_elmer2000@yahoo.com